Final Report

Beaufort Sea Nearshore Under-Ice Currents: Science, Analysis and Logistics

by

Thomas J. Weingartner
Stephen R. Okkonen

Institute of Marine Science
University of Alaska Fairbanks
Fairbanks, AK 99775-7220

weingart@ims.uaf.edu
okkonen@alaska.edu

December 2001

Table of Contents

List of Tables

List of Figures

Abstract

We measured velocity, temperature, salinity, and transmissivity (a proxy for suspended sediment load) hourly for one year within the landfast ice zone of the Beaufort Sea near Prudhoe Bay, Alaska. The purpose was to measure under-ice and open water currents for evaluating oil-spill trajectories and sedimentation risk in this nearshore environment. The measurements were made from an array of three instrumented moorings spanning an along-shore distance of ~28 km within the western portion of Stefansson Sound. The circulation dynamics vary seasonally and in response to the formation and disappearance of the landfast ice. The landfast ice formed in mid-October 1999 and remained intact until the end of June 2000. Current speeds were typically about 3 cm s^{-1} and most of the current variability was at subtidal periods. Current speeds greater than 10 cm s^{-1} were observed less than 5% of the time at two locations and about 10% of the time at one location. During the open water season, current speeds typically exceeded 10 cm s^{-1} and the maximum currents were greater than 10 cm s^{-1}. Winds and currents were strongly correlated during the open water season but uncorrelated once the landfast ice was established. The highest transmissivity signals were observed in early October 1999 during a strong gale and in early June, when the landfast ice was still intact and winds were weak. We believe that the June turbidity signal was associated with the summer freshet from the Sagavanirktok River, which flows beneath the landfast ice and (at least) 10 km offshore of the river mouth.

These data represent the first year-round (including the freeze-up and ice melt seasons) current measurements for this area. This information is critical for designing oil spill response protocols for offshore drilling operations specifically at the nearby Northstar and Liberty fields and generally for similar landfast ice regions of the Alaskan Beaufort Sea. The data should also be useful in evaluating regional numerical circulation models that would be used for oil spill trajectory predictions. While these were the principal reasons for this study, the data will have broader scientific applications relevant to other arctic shelves. For example, the low current energy beneath the landfast ice zone implies little vertical mixing, which has important implications for the fate of river waters entering the shelf in early summer. Consequently, this data will lead to a better understanding of mixing processes and circulation on the innermost portion of arctic shelves.

Background and Relevance to Framework Issues

Within the vicinity of Prudhoe Bay, the Northstar oil field is being developed and the Liberty prospect is under construction for further development. Both prospects lie offshore and there is some concern that development might impact nearshore biota. The Minerals Management Service (MMS) Alaska OCS Region expects that these concerns will require integrated studies of key issues including long term impacts on benthic/kelp communities and other sensitive resources.

Understanding the under-ice currents is a necessary precursor to estimating potential effects of oil spills on sensitive resources in the landfast ice zone, and in particular at the Liberty project. The landfast ice zone typically lies shoreward of the 20-m isobath [Reimnitz 1978]. Such spill trajectory assessments cannot be modeled with the standard MMS oil spill trajectory analysis based on regional circulation. Detailed under-ice current measurements are necessary. Another important question is whether the under-ice currents could transport suspended sediments from the development area to the nearby Boulder Patch, and endanger kelp during the critical under-ice growth period.

1

Under-ice current speed and direction are important because currents of 10–20 cm s^{-1} will move spilled oil along the underside of the ice. The one study of under-ice currents supported by MMS [reported by Matthews 1981] was made within Stefansson Sound. Matthews did not measure the under-ice currents directly but rather inferred them from near-bottom measurements with assumptions that the flow field was unstratified and that two-dimensional mass balance held. He inferred that under-ice currents averaged 6 cm s^{-1} and had a maximum velocity of 35 cm s^{-1} directed onshore. The latter speed is more than sufficient to move oil beneath the landfast ice. Indeed, if these currents are sustained they imply onshore displacements of about 3 and 20 nmi d^{-1}. Matthews found that average currents under landfast ice appeared to be related to brine drainage from growing sea ice and that the highest currents were associated with wind-forced, negative surges. Along-shore currents appeared to have similar magnitudes. Our expectation is that wind-forced currents should dominate in this region, as tidal currents are about 4 cm s^{-1} [Kowalik and Proshutinsky 1994].

Matthews' [1981] measurements, made from mid-November 1978 through February 1979, were obtained within Stefansson Sound, a shallow lagoon bounded offshore by barrier islands. We anticipate that the lagoon circulation is less energetic than the flow offshore of the barrier islands. In this regard, his measurements are probably more applicable to the Liberty development than to Northstar. Moreover, his measurements did not include the early fall period of vigorous ice growth and the developing landfast ice cover. We expect under-ice currents to be swifter during this period as the ice is still mobile and therefore effective in transmitting momentum from the winds to the underlying ocean. We expect that until the landfast ice cover is established, the drag of the ice over the ocean will impart momentum into the ocean via a frictional boundary layer (e.g., very large vertical gradients in ocean velocity) near the surface. Once formed, the landfast ice is an immobile lid that inhibits the flux of wind energy into the water column. *A priori* we expect that the portion of the inner shelf covered by landfast ice will be relatively quiescent. Finally, Matthews' measurements did not include the period of river runoff, which increases rapidly in early summer when the landfast ice is still present. This region receives a large and sudden influx of river water (primarily from the Sagavanirktok River), with much of the discharge probably flowing under the landfast ice [Carmack et al. 1989; Dean et al. 1994]. Whether this fresh water mixes with ambient shelf water and, if it does, how this mixing evolves, is crucial in the seasonal evolution of the nearshore and shelf circulation [Chapman and Lentz 1994*;* Yankofsky and Chapman 1997; Weingartner et al. 1999]. The river plume will spread under the ice, possibly forming strong vertical velocity gradients with maximum speeds near the bottom of the ice.

Goal and Objectives

The goal and objectives of this project were to provide direct measurement of winter under-ice and open water currents in the vicinity of the Liberty and Northstar projects to help MMS and the Alaska Department of Environmental Conservation evaluate oil-spill and sedimentation risk to the nearshore Beaufort Sea, including the Boulder Patch and other local resources. The specific objectives were to:

1. Deploy three instrumented moorings in the vicinity of the Liberty and Northstar projects for a period of one year (Figure 1). The moorings collected velocity, temperature, salinity, and one collected transmissivity data. Transmissivity is a proxy for the suspended sediment load in the water column. Our moorings were deployed in the western end of Stefansson Sound—west, east and offshore of the Sagavanirktok River delta.

2. Analyze the current meter and local wind records to quantify the magnitude of current and wind variability and their relationship to one another.

3. Determine the vertical structure of the currents throughout the water column and how this structure changes with the development of the landfast ice through winter and in summer when the ice melts and rivers flood the inner shelf.

Tables 1 and 2 summarize details on the mooring nomenclature, locations, measurement period, and bottom depths and instrumentation used. Mooring McClure was within the region of the extensive kelp beds known as the Boulder Patch. Currents at each location were measured with a 1200 kHz acoustic Doppler current profiler (ADCP) which collects backscattered sound integrated over 0.5-m depth bins throughout the water column and to within about 1.0 m beneath the ice. These instruments transmit sound at 1200 kHz and then measure the Doppler shift of the backscattered signal. The ADCPs depend upon water column scatterers (density discontinuities, plankton, and suspended matter). Internal software reconstructs the current profile throughout the water column at a high vertical and temporal resolution. The ADCPs were mounted on gimbals in a non-ferrous plastic frame, which ensured that the instrument was vertically oriented throughout the measurement period. The transducer head for each ADCP was located about 0.85 m above the bottom. Valid velocity measurements were acquired above the moorings at 0.5-m intervals beginning at 1.0 m (1.5 m at Argo) above the ADCP transducer head. Due to interference from transducer beam sidelobes, the shallowest valid velocity measurements were acquired at about 1 m below the open-water surface or ice-bottom surface. In the following discussion, the shallowest measurements are referred to as shallow-bin measurements and the deepest as deep-bin measurements (the deep-bin measurements were acquired at ~2.35 m above bottom at Argo, and ~1.85 m above the bottom at Dinkum and McClure). Temperature, salinity, and water pressure were measured with a MicroCAT (manufactured by Sea-Bird Electronics, Inc.) at station Argo. Temperature, salinity, and transmissivity were obtained from SEACATs (manufactured by Sea-Bird Electronics, Inc.) at stations McClure and Dinkum. All of these variables were sampled at half-hour intervals from sensors located about 0.5 m above the bottom. However, due to an error in setting the sampling rate for the McClure SEACAT, only four days of data were acquired at this mooring. These data are not presented in this report. The mooring deployment period was 382 days in length.

Wind speed and direction measurements at the Deadhorse airport were available for the period from 19 September 1999 to 13 September 2000. The sampling rate was variable, but typically once per

hour. The wind record was interpolated to hourly intervals for comparison with the current meter records.
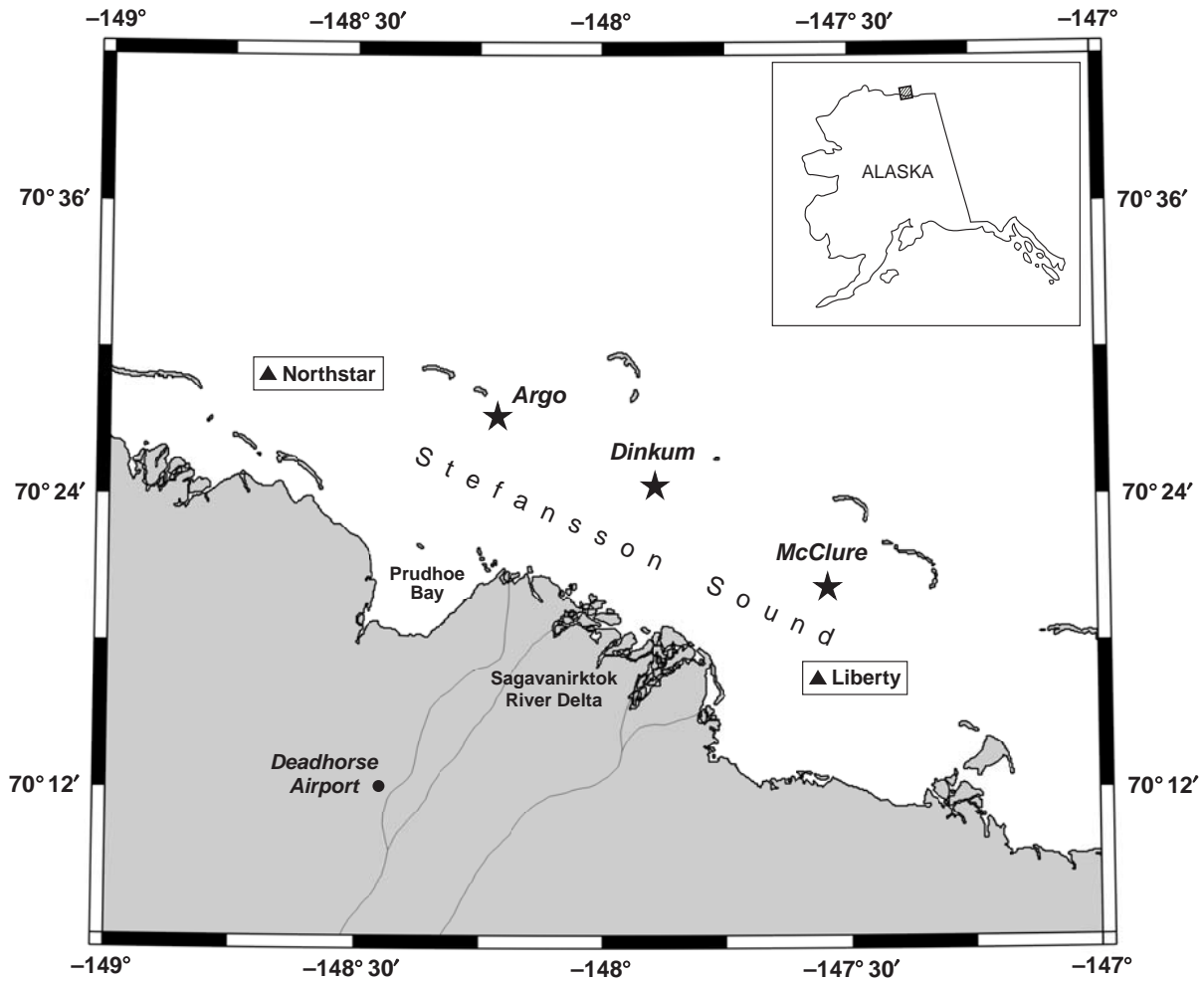
Figure 1. Map of Prudhoe Bay and Stefansson Sound, Alaska with the location of the three mooring sites—Argo, Dinkum, and McClure—indicated.

Table 1. Mooring specifics.

Mooring	Latitude (N)	Longitude (W)	Time Deployed (1999, GMT)	Time Recovered (2000, GMT)	Bottom Depth

Argo	70° 27.177′	148° 12.722′	13 Aug, 1821	1 Sep, 0556	8.4 m
Dinkum	70° 24.352′	147° 53.656′	14 Aug, 1837	1 Sep, 0318	6.8 m
McClure	70° 20.204′	147° 32.701′	14 Aug, 2007	1 Sep, 0054	6.7 m
Deadhorse Airport	70° 11.7′	148° 27.7′	19 Sep	13 Sep	

Table 2.   Mooring instrumentation. Each of the ADCPs was situated about 1 m above the seabed and the SEACATs and MicroCAT were situated about 0.5 m above the seabed.

Mooring	Data Analysis Period	Instrument	Variable Measured
Argo	19 Sep 99 – 1 Sep 00	1200 kHz ADCP	current velocity
Argo	″ ″	MicroCAT	temperature, salinity and water pressure
Dinkum	″ ″	1200 kHz ADCP	current velocity
Dinkum	″ ″	SEACAT	temperature, salinity and transmissivity
McClure	″ ″	1200 kHz ADCP	current velocity
McClure	″ ″	SEACAT	temperature, salinity and transmissivity
Deadhorse	″ ″	Anemometer	wind speed and direction

Results

Currents and winds

Mean statistics for the currents and moorings are summarized in Table 3. All statistics are based on the common time period of 0000 on 19 September 1999 to 0000 on 1 September 2000 (GMT). The principal axes calculation shows that most of the flow variability ($> \sim 90\%$) at all mooring sites is oriented along the length of Stefansson Sound, e.g., the flow is predominantly along the northwest–southeast axis. Thus flow variations in the cross-sound direction are relatively weak. The winds are also strongly rectilinear, with 90% of the wind variability oriented along the east–west axis. While the mean current velocities are small the variability about the mean is large. The variance changes with the ice cover. Standard deviations during the open water period are 3–6 times greater than during the ice covered period. The integral time scales, τ, of the current and winds are similar, with each being about three days. This is the decay time scale for flow (and wind) events and it is the time required to gain a new "degree of freedom" from a record of N data points. We use it to estimate the effective number of degrees of freedom [Davis 1976] in our data set, which is defined as $N_{eff} = N\Delta t/\tau$, where Δt is the sampling interval.

Table 3. Currents and winds summary statistics. The current statistics are given for a depth about 1.5 m above each instrument.

Mooring	Net Velocity		Principal Axis of Variance					
	Speed (cm s^{-1})	Direction (°T)	Variance Explained %	Direction (°T)	Max Speed (cm s^{-1})	Integral Time Scale (days)	Mean±SD North–South Velocity (cm s^{-1})	Mean±SD East–West Velocity (cm s^{-1})
Full Record								
Argo	4	278	97	97	99	3	0 ± 3	−3 ± 14
Dinkum	2	305	96	119	114	3	1 ± 8	−2 ± 4
McClure	2	2	90	151	82	3	2 ± 11	0 ± 7
Deadhorse winds	1.3 (m s^{-1})	250	90	77	25 (m s^{-1})	3	−1 ± 5 (m s^{-1})	−2 ± 12 (m s^{-1})
Landfast Ice Period								
Argo	2	283	88	99	24	3	0 ± 2	−2 ± 6
Dinkum	0	–	83	145	18	2	0 ± 4	0 ± 3
McClure	1	12	82	173	15	3	1 ± 4	0 ± 2
Open Water Period								
Argo	3	270	97	97	99	4	0 ± 14	−3 ± 18
Dinkum	2	322	95	119	114	4	2 ± 11	−1 ± 18
McClure	2	360	95	150	82	4	2 ± 13	0 ± 9

Figure 2 shows time series of the current from the bin about 1.5 m above the ADCP with wind components projected onto their principal axes. Each of the current meter time series in this figure was low-pass filtered to suppress tidal motions. The wind time series was smoothed with a 25-hour running mean. The time series show that the current variations are seasonally modulated, with most of the variance and the highest current speeds occurring from July through October. The current variance between mid-October and the end of June is a factor of 5–10 times smaller than the variance prior to and after these dates. As shown below, this is the time period when we believe that landfast ice was established in the sound. Flow events exceeding 25 cm s^{-1} are common prior to mid-October 1999 and after 1 July 2000, but between these dates flow speeds seldom exceeded 10 cm s^{-1}. The mid-October through June period is highlighted in Figure 3, which shows the *unfiltered* current time series at the three mooring sites. Although the currents are comparatively weak, there are several events in winter, each of several days duration, when the flow is quite persistent. For example, beginning in late December, there is a 5-day event when current speeds averaged about 10 cm s^{-1} at all locations. Such events can transport suspended material over a distance of more than 40 km.

Inspection of the current time series in Figures 2 and 3 suggests that these are all well correlated with one another throughout the record. Quantitatively this is supported by the results of an empirical orthogonal function (EOF) analysis (based on the correlation matrix) on the current components aligned along their principal axes. The first EOF mode accounts for 92% of the variance while the second and third modes are not significant, following North et al.'s [1982] procedure. The dominance of the first EOF mode implies that flow variations along Stefansson Sound are coherent over spatial scales of at least 28 km. The results also suggest that a single mooring would suffice in capturing along-shore flow variations in this region.
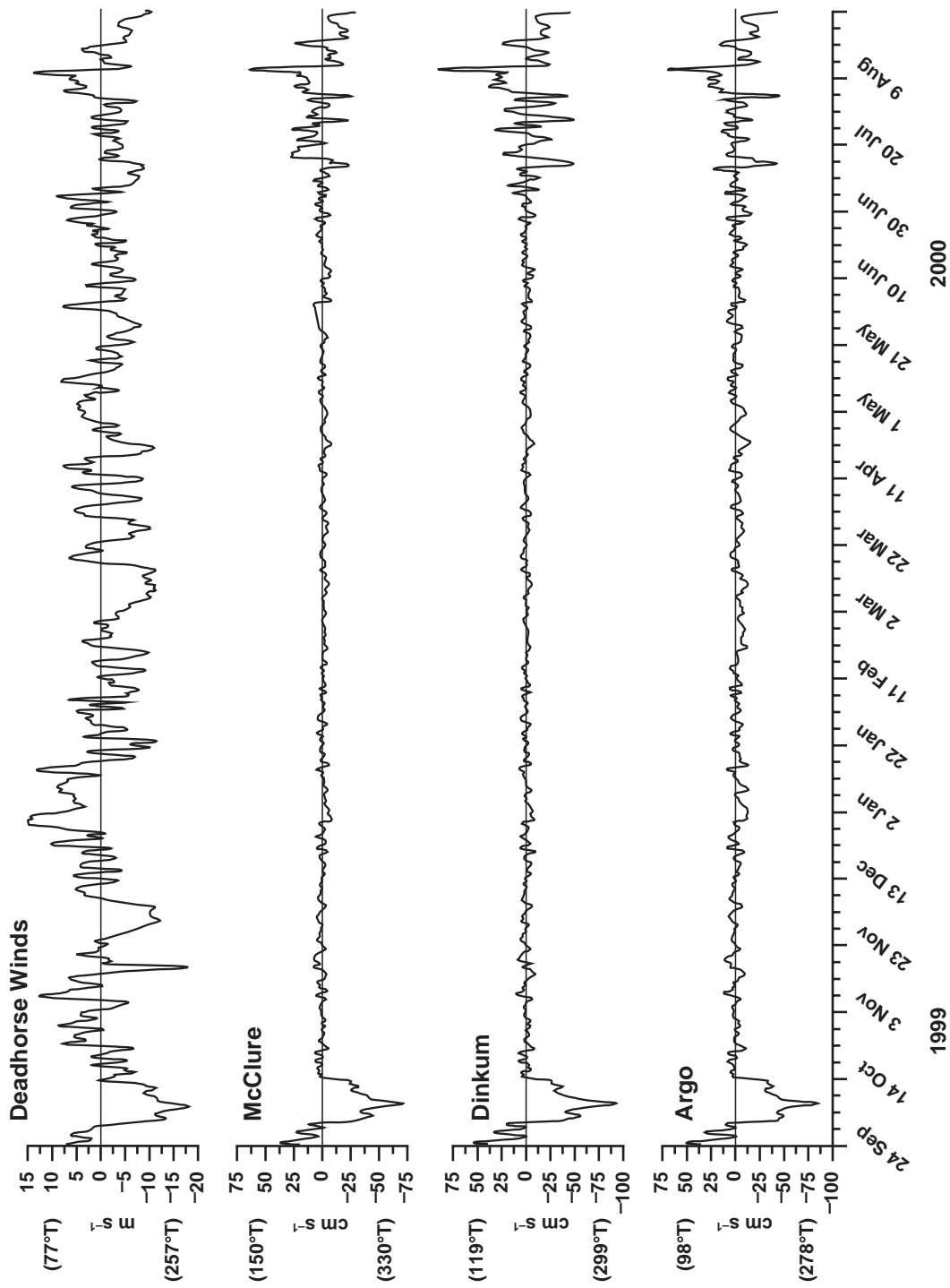
Figure 2. Winds and currents projected along their principal axis of variance. The direction of the positive and negative values at each location is indicated along the ordinate. The currents were low-pass filtered to suppress diurnal and semi-diurnal tidal fluctuations. The winds were smoothed with a 25-hour running mean.
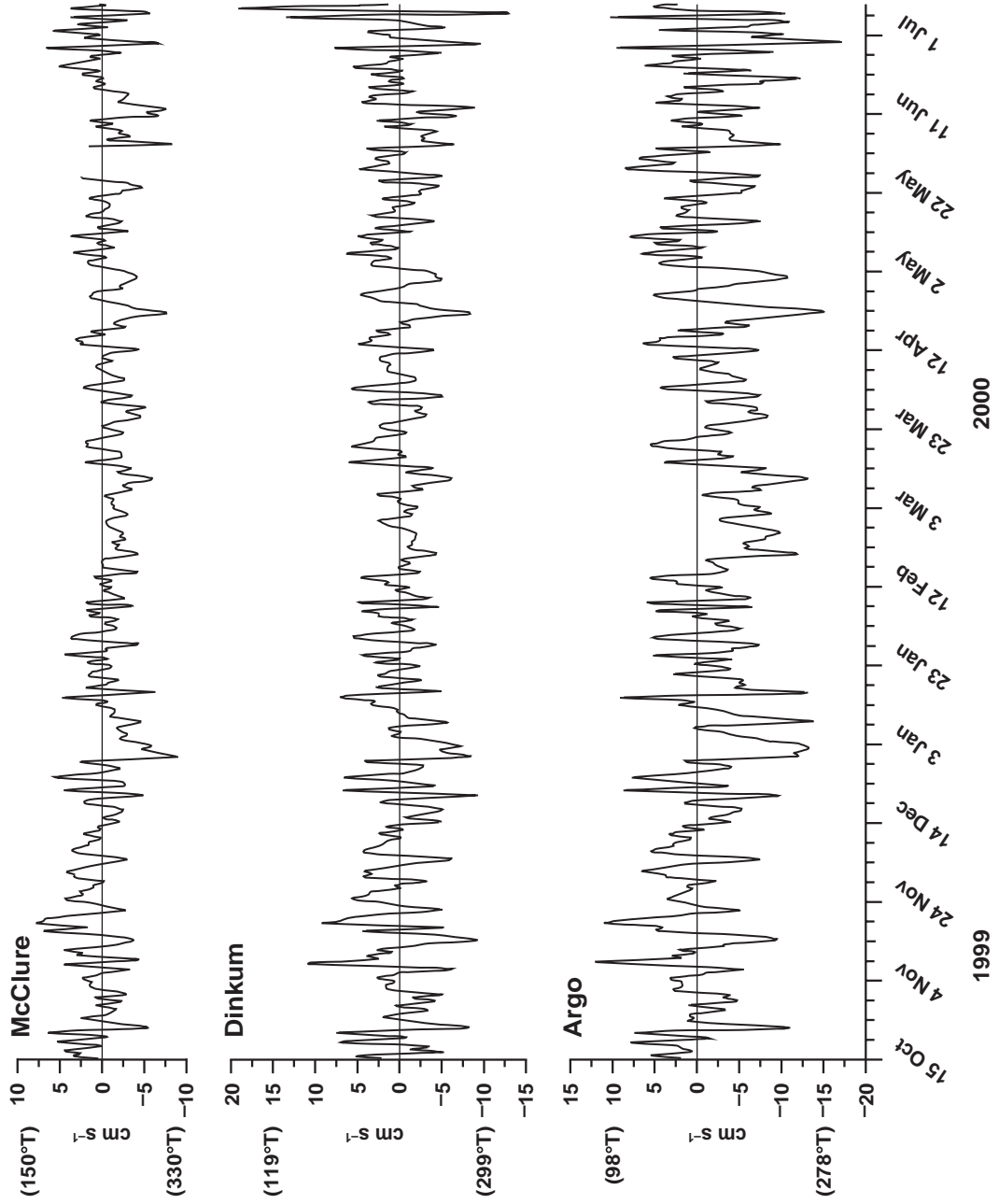
8

Figure 3. Time series of (unfiltered) currents projected along their principal axis of variance during the landfast ice period.

We next consider how the velocity and current shear vary with the seasonal formation of the landfast ice. Figure 4a shows 5-day running mean estimates of the sea ice thickness as determined from the ADCP. The thickness B was estimated as the difference between the bottom depth Z (Table 1), and the sum of the height of the transducer above the bottom H and the range from the transducer at which the intensity of the reflected acoustic signal was maximum R (e.g., $B = Z - [H + R]$). The uncertainty in the thickness measurement is ± 0.25 m because the ADCP integrates over a 0.5 m layer. Sea ice appears in early October and steadily increases to a thickness of ~1.5–2.0 m by mid-March. Ice thickness remains constant through mid-June but then rapidly ablates and is completely gone by mid-July. (Floating sea ice is probably present prior to mid-October and after breakup in July, but the exact dates at which sea ice first appears and then completely disappears cannot be unequivocally determined from the ADCP data.) Figure 4b shows time series of the bottom-tracking mode. For ADCPs deployed in an upward-looking orientation, the bottom-tracking mode provides measurements of sea ice drift speed and direction when sea ice is present. In the absence of ice, surface current speeds will not be accurate because of sidelobe contamination. The bottom-tracking mode shows that the near surface, including the ice, is in motion until mid-October, at which point the bottom-tracking speeds fall to zero and remain there until the end of June (when the ice thickness is ~0.5 m). In aggregate, these figures suggest that the period of landfast ice lasts for about eight and one-half months. Figure 4c shows the difference in speed (or current shear $d|\mathbf{V}|/dz$, where $|\mathbf{V}|$ is the speed and z is the depth coordinate) between the shallowest depth bin beneath the ice or sea surface and the deepest depth bin. At Dinkum the depth range over which these differences are computed is ~4 m during open water periods and ~2 m during maximum ice thickness. Current speeds typically differ by about 5 cm s^{-1} over the measured depth range when landfast ice is present. However, shears can be quite large when the ice is absent, with differences of up to 80 cm s^{-1} observed. But more typically the differences are between 20 and 30 cm s^{-1}. Finally, Figure 4d is the unfiltered velocity time series, which shows that the largest current speeds and greatest current variance occur before the landfast ice is established and after it breaks up. The frequency distribution of the variance also changes seasonally. For example, approximately 80% of the variance is subtidal (periods longer than 30 hours) during the landfast ice period, while more than 90% of the variance is in the subtidal periods during the open water period.

We conclude this section with the seasonal speed histograms shown in Figure 5. The left-hand plot shows histograms of current speed during the landfast portion of the year and the right-hand panel shows histograms for the open water ice period. For the latter period, the majority of current speeds are less than 10 cm s^{-1} at all locations, while during the remainder of the year the majority of the current speeds exceed 10 cm s^{-1}. For example, at Argo, 10.5% of the current speeds exceeded 10 cm s^{-1} during the landfast ice period. At Dinkum and McClure the comparable values were 2.4% and 1.3%, respectively. Matthews [1981] inferred from continuity arguments that under-ice current speeds could be as large as 35 cm s^{-1}. In contrast, our direct current measurements suggest that under-ice current speeds exceed 10 cm s^{-1} less than 10% of the time.
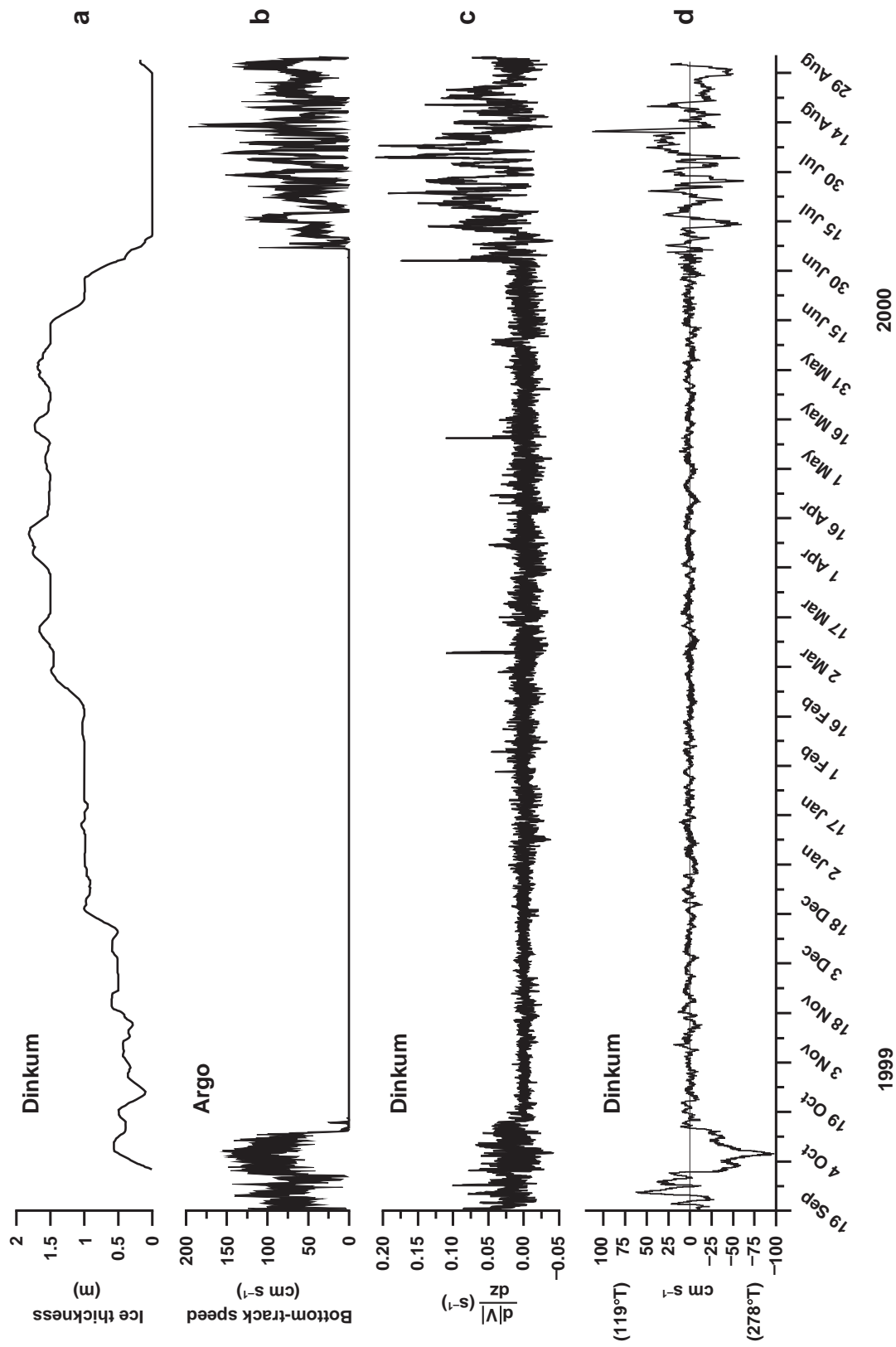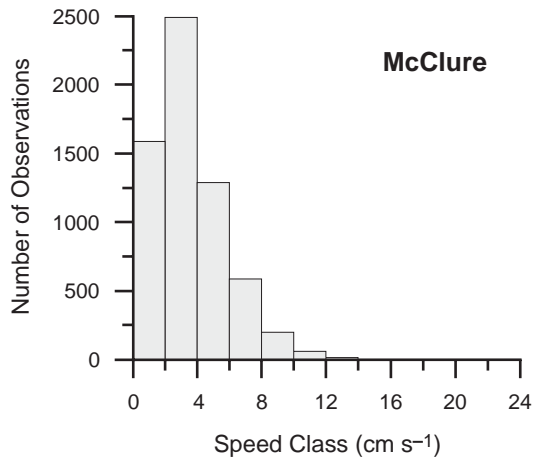
Figure 4. Time series of a) ice thickness (smoothed with a 5-day running mean) at Dinkum, b) bottom-track speed, c) vertical shear of the current speed, and d) unfiltered currents along the principal axis. All measurements are from Dinkum except the bottom track speed, which is from Argo.
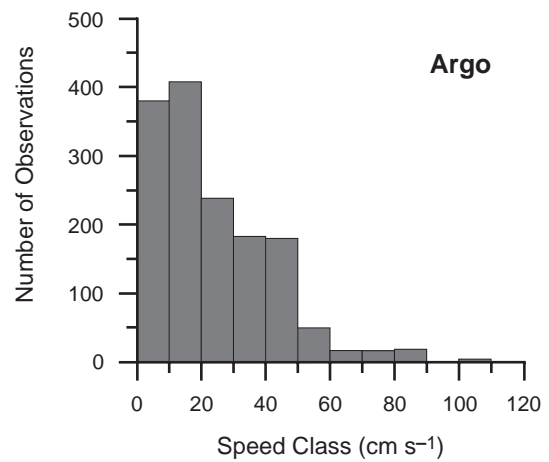
11

Landfast Ice Period

Open Water Period

McClure

McClure

Dinkum

Dinkum

Argo

Argo

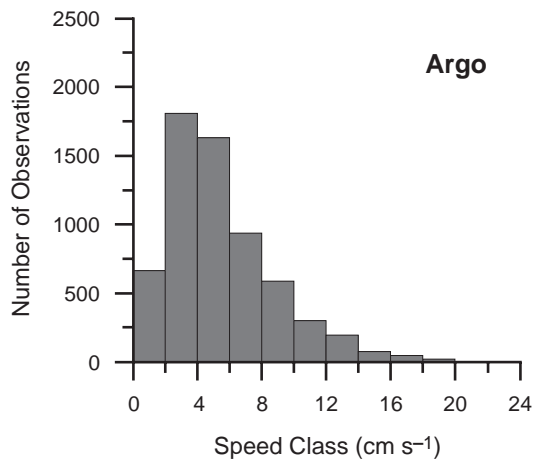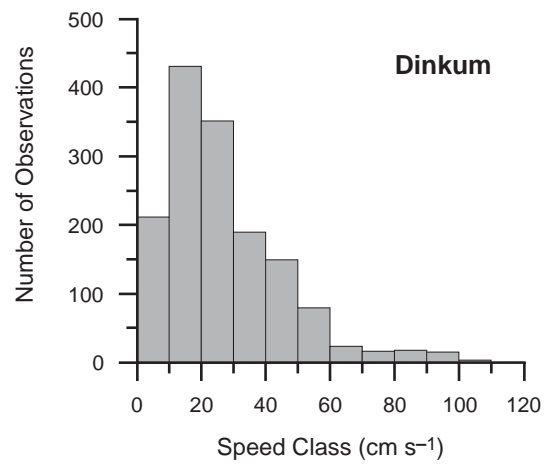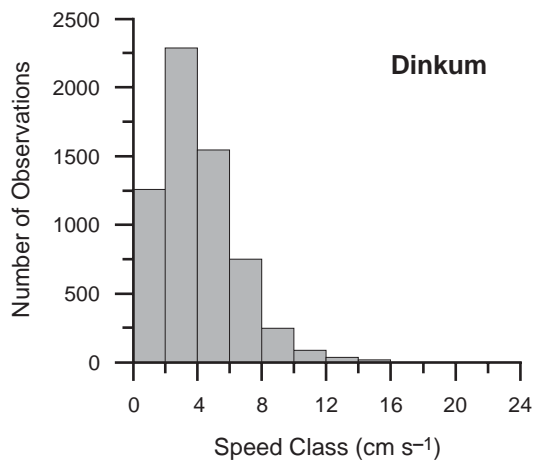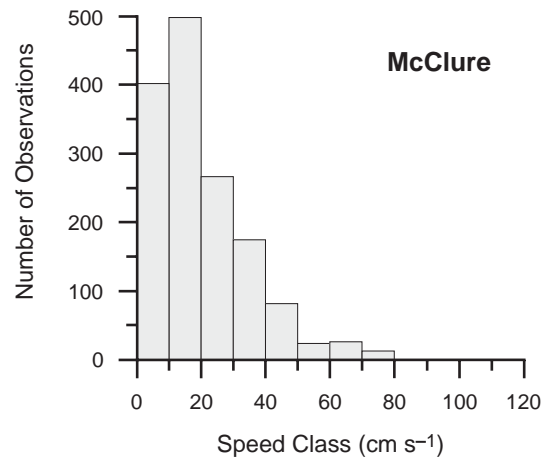Number of Observations

Speed Class (cm s⁻¹)

Figure 5. Histograms of current speed during the landfast ice (left-hand plot) and open water periods (right-hand plot).

Wind and current correlations

The landfast ice is a rigid, immobile cover that should effectively decouple the ocean from the direct effects of wind stress. Consequently the correlation between the winds and the currents should be different between the open water and ice-covered periods. This is in fact the case, as shown by cross-correlation analysis (Table 4) between the wind and current components projected onto their principal axes. Cross-correlation analyses of Deadhorse winds and currents at the three mooring sites were computed for: 1) the open water/drifting ice period from 19 September 1999 through 14 October 1999, 2) the landfast ice period from 15 October 1999 through 30 June 2000, and 3) the open water/drifting ice period from 1 July 2000 through 31 August 2000 (Table 4). The results show that currents are significantly correlated with the prevailing winds at lags of one or two hours during the periods of open water/drifting ice at all mooring locations. The higher correlations associated with the earlier open water period are likely attributable to the nearly two-week period of strong east–northeasterly winds in early October. Correlations associated with the landfast period are not statistically significant at all locations. Thus, the results are consistent with the frictional decoupling of the wind from the water by the landfast ice. The behavior of the flow under the landfast ice differs markedly from that observed under freely-drifting ice, as shown for the Beaufort shelf by Aagaard [1984] and the Chukchi Sea by Weingartner et al. [1998]. At these locations the winter, under-ice flow can be strong and is strongly correlated with the surface winds.

Table 4. Cross-correlation between winds and currents. Values denoted by an asterisk are significant at P = 0.01. N_{eff} is the effective number of degrees based upon an integral time scale of 3 days.

Mooring	19 Sep 99 – 14 Oct 99 $N_{eff} = 9$	15 Oct 99 – 30 Jun 00 $N_{eff} \sim 86$	1 Jul 00 – 31 Aug 00 $N_{eff} \sim 21$
Argo	0.94* (1 hr)	0.09	0.70* (5 hr)
Dinkum	0.94* (2 hr)	−0.02	0.73* (5 hr)
McClure	0.94* (1 hr)	−0.13	0.74* (4 hr)

Temperature, salinity, and transmissivity

Water property parameters also vary considerably throughout the year. The annual ranges in temperature (T) and salinity (S) are shown in Figure 6, which is a scatterplot or TS-plot of daily temperature and salinity values at Argo and Dinkum. Salinity ranges from 20–35 psu and temperatures range between 4 to approximately –1.7° C. In general, low salinities are associated with high temperatures and high salinities with low temperatures. The solid line in the TS-plot is the freezing point curve as a function of salinity. Many of the observed values fall on this line or slightly above it as might be expected in these shallow areas. We also note that because the MicroCATs and SEACATs were re-deployed upon recovery we could not post-calibrate these instruments. The cluster of points on the freezing point provides one indication that the sensors maintained their calibrations at least through most of the year.
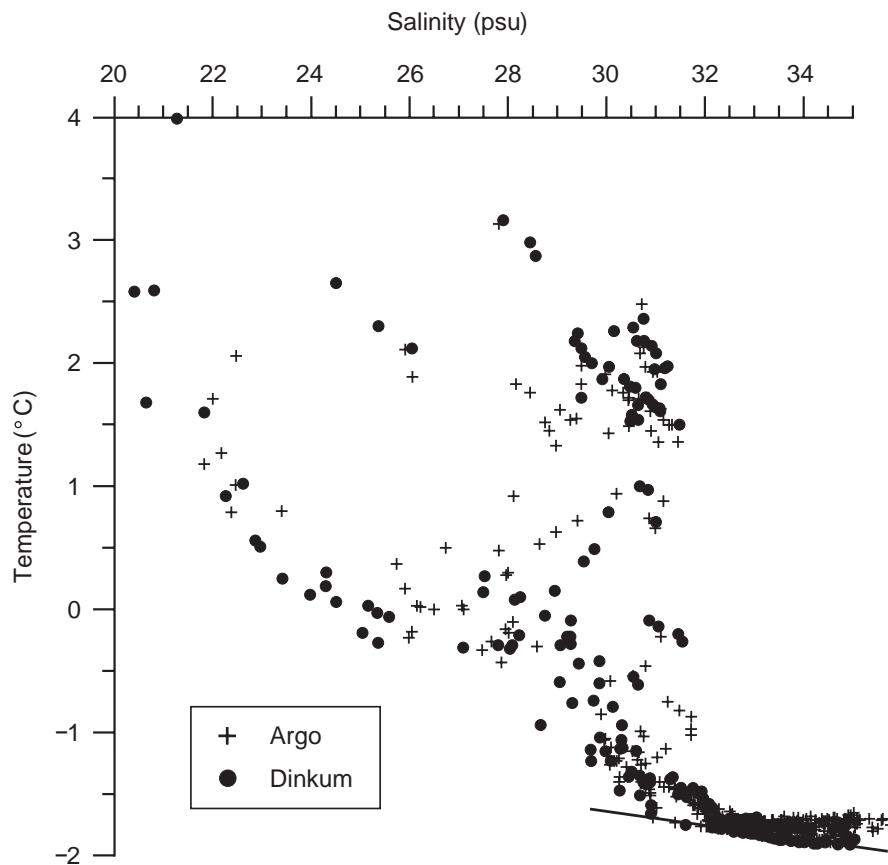

Figure 6. Scatterplot of daily temperature and salinity values at Argo and Dinkum.

14

The seasonal variation in water properties is seen in Figure 7, which shows time series of a) ice thickness, b) temperature, c) salinity, and d) transmissivity. Temperature decreases rapidly from late September through mid-October. It remains at the freezing point (approximately $-1.7°$ C) until late June, whereupon it slowly increases to about $0°$ C by late July. At that time there is a rapid increase to $4°$ C before decreasing to about $0°$ C by the end of the record. Salinity varies between 28 and 32 psu prior to the establishment of the landfast ice in mid-October and then increases to 34–35 psu by January. This increase is related to the formation of sea ice, which expels salt as it forms. Thereafter, salinities vary between 33 and 35 psu throughout the remainder of winter and then slowly start to decrease in June. The temperature increase and the associated drop in salinity beginning in late June and continuing through July coincide with the ablation and breakup of sea ice and probably also reflect the addition of fresh water to the system due to river runoff. In August, salinity decreases and temperature increases very rapidly. We suspect that this sudden freshening (a salinity decrease from about 28 to 20 psu) and warming is associated with the mixing of river water throughout the water column, as these coincide with the strong current shears observed in early August (Figure 4c). These shears were associated with the strong westerly winds of early August (Figure 2), which should enhance vertical mixing of a stratified water column. Assume that the ~7-m-deep water column in Stefansson Sound can be approximated as a two-layer system with the river plume at the surface, having an unknown thickness but with a presumed salinity of 5 psu. The lower layer has a salinity of 28 psu (as observed before the rapid salinity decrease in early August). Mass balance considerations suggest that the plume thickness is about 2.5 m. (For plume salinities of 10 and 0 psu, the plume thicknesses are 3 and 2 m, respectively.) We suspect that the water column begins to stratify in June when North Slope rivers breakup. River plumes have been observed under the landfast ice at this time of the year where they establish strongly stratified conditions [Carmack et al. 1989; MacDonald et al. 1989; Dean et al. 1994]. Our experimental design precluded obtaining the vertical gradients of salinity and temperature needed to unequivocally establish that river water is present beneath the ice and above our mooring. Searcy et al. [1996] show that under-ice river plumes can strongly affect the summer breakup of landfast ice.
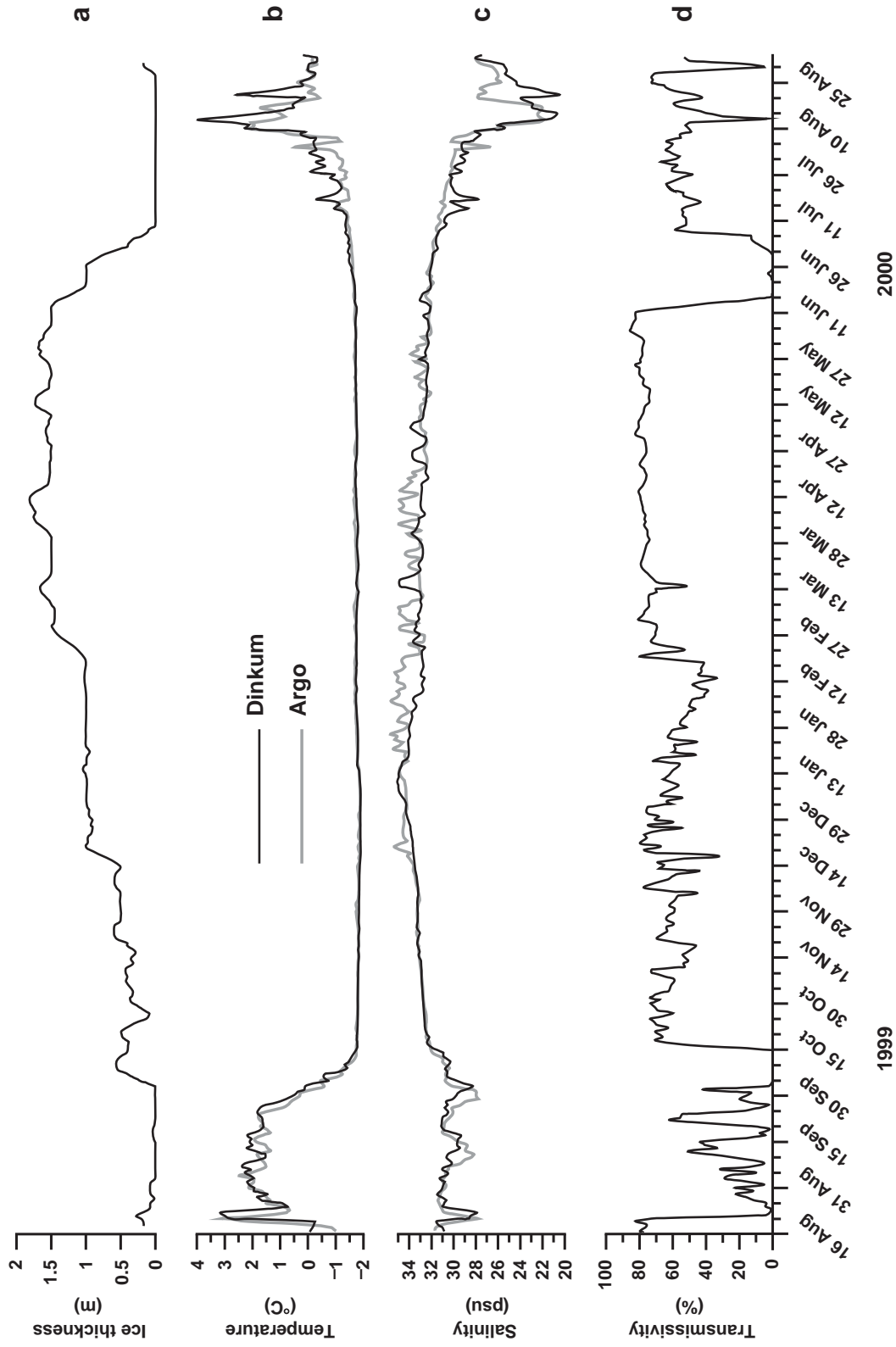
Figure 7. Time series of a) ice thickness, b) temperature, c) salinity, and d) transmissivity.

16

Transmissivity is a relative value that is proportional to the amount of suspended material in the water column. (Additional measurements would be needed to relate transmissivity to suspended load.) It, too, shows a strong seasonal cycle. Transmissivity is relatively high (low suspended material) in winter and low in summer and fall when the lagoons are ice free and/or covered with drifting ice. Interestingly, transmissivity dropped to very low levels in mid-June when the landfast ice was intact but melting rapidly. Current speeds and shear were also low at this time. There are several possible sources of suspended material that contributed to the low transmissivity: The first is sediment that was incorporated into the ice during the previous fall freeze-up and which drops out when the ice melts. The second is ice algae flushed from the ice during melt. The third is sediment carried by river plumes flowing under the ice but above the depth of mooring. Conceivably this suspended material drops out as the river plume flows offshore under the ice. The fourth is sediment scoured from the bottom from a nearby "glory hole". While all of these sources could be contributing simultaneously, we believe that the latter two are most likely since the low transmissivity signal occurs during the period of maximum increase in river discharge from the Sagavanirktok River at Pump Station 3. The mean daily Sagavanirktok River discharge for 1 May 2000 to 30 September 2000 is shown in Figure 8. Discharge is negligible through May, increases rapidly over the first week of June and attains a peak of ~700 $m^3 s^{-1}$ on 9 June. Discharge then falls off rapidly by late June and remains relatively constant at ~150 $m^3 s^{-1}$ through August. Note that the peak discharge on 9 June precedes by two days the rapid decrease in transmissivity (increase in suspended sediment load) observed at mooring Dinkum on 10 and 11 June (Figure 7). In fact, the vertical velocity structure also changes as the discharge peaks. This is evident in Figure 9, which shows time series of the discharge, ice thickness, transmissivity, vertical velocity differences, and velocities beneath during the May–June 2000 period at the Dinkum mooring. Both components of the velocity shear increase as the discharge peaks. The increase in shear suggests a two-layer structure in the water column. There is also an increase in the cross-shore velocity consistent with the offshore spreading of the plume. The acoustic backscatter signal (not shown) suggests an increase in backscatter intensity at about 1.5 m beneath the ice. This is consistent with the estimates made above based on salinity changes for the plume thickness. The increase in backscatter intensity at this depth is presumably related to the density difference between the river plume and seawater and/or the (presumed) increase in suspended material within the plume. All of these changes coincide with the rapid increase in discharge and its presumably high sediment load. Note also that following the peak discharge the ice began to thin rapidly. Presumably this decrease is related to the relatively warm water associated with the river plume. River plume temperatures should be at least 1.5° C to 2.0° C above the melting point of sea ice. Searcy et al. [1996] estimate that rivers might provide up to one-third of the heat required to melt landfast ice in the vicinity of river mouths.
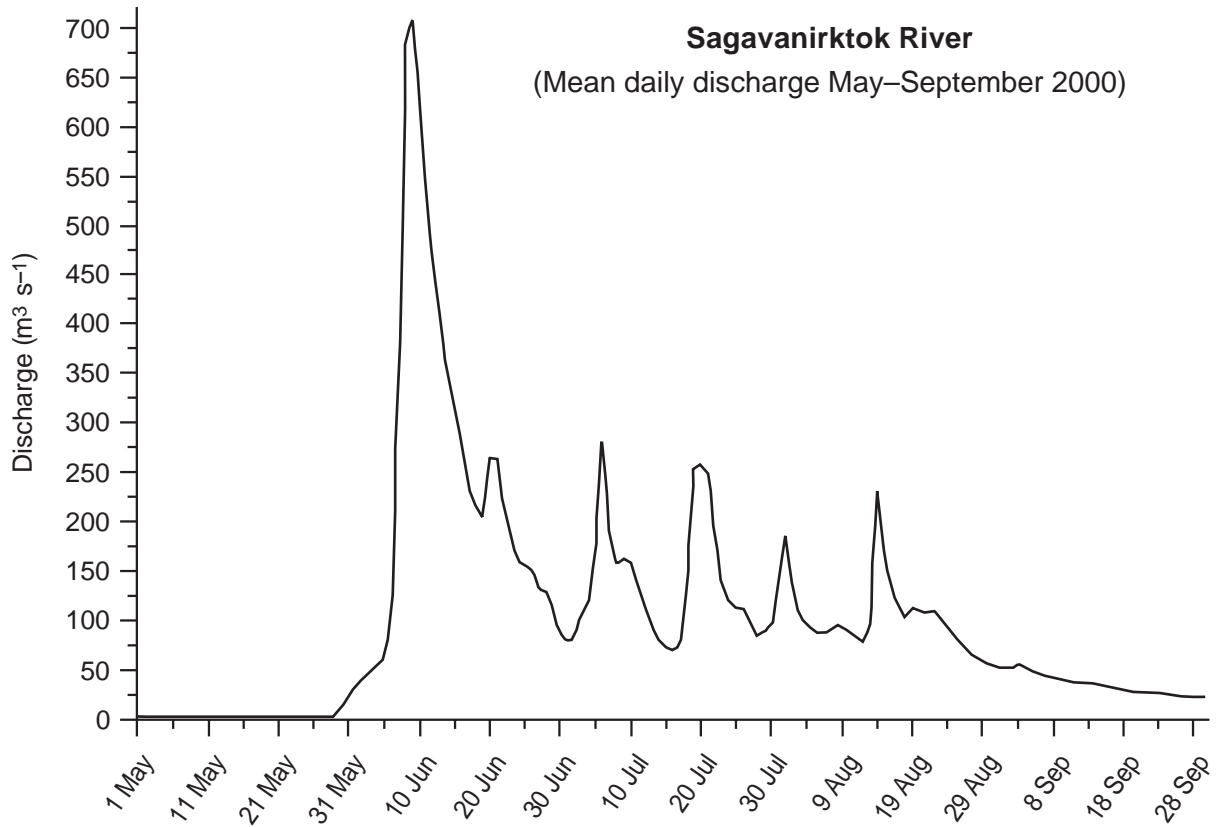
Figure 8. Mean daily discharge from the Sagavanirktok River for May–September 2000 based on USGS discharge records collected near Pump Station 3 (60.015°N, 148.75°W). The maximum daily discharge occurred on 9 June 2000.
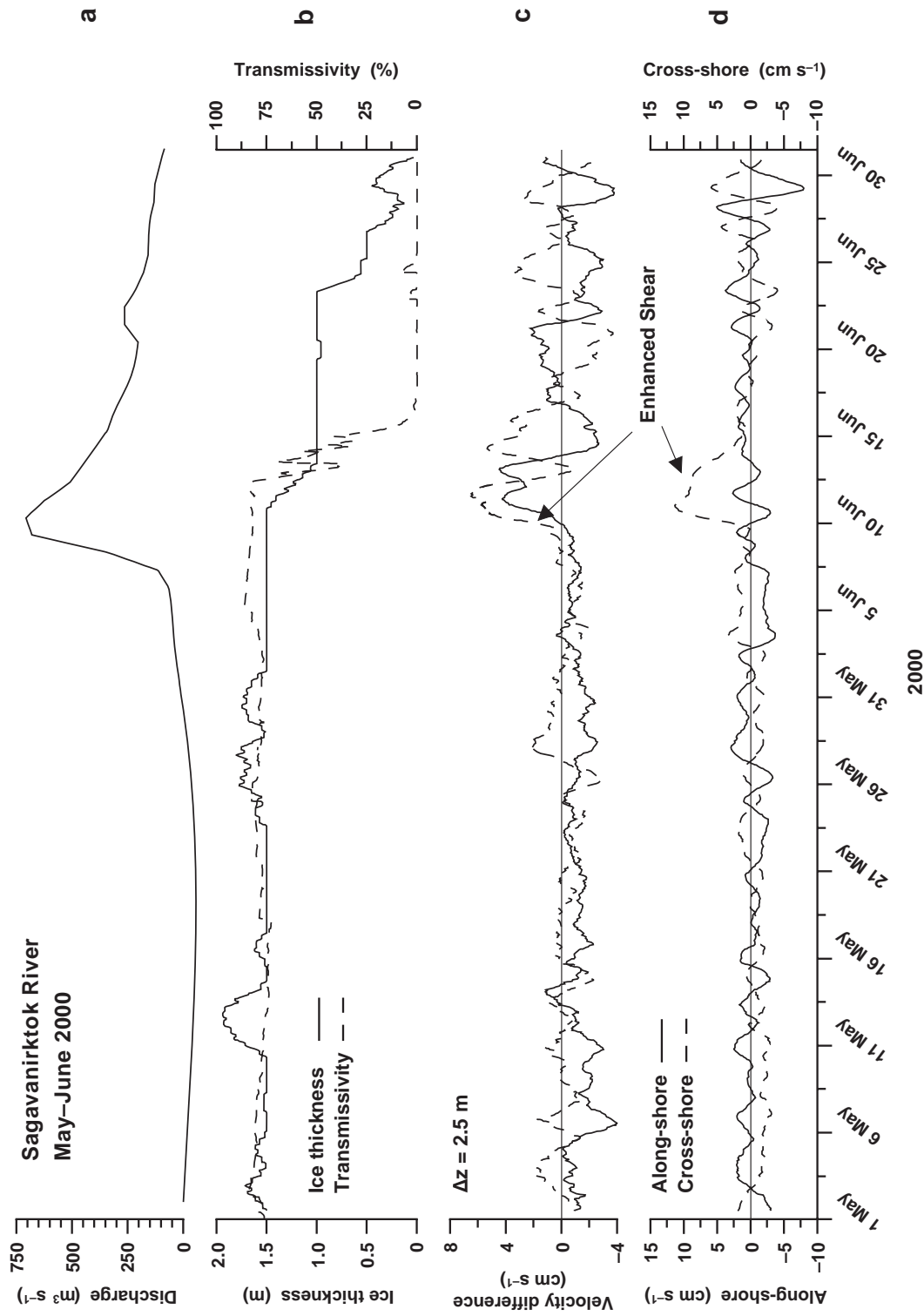
Figure 9. Time series for May–June 2000 of a) mean daily discharge from the Sagavanirktok River, b) ice thickness (solid line) and transmissivity (dashed line), c) velocity difference (shear) for the along-shore and cross-shore velocity components, and d) the along- and cross-shore velocity. The oceanographic data were from mooring Dinkum. Solid lines depict the along-shore components and dashed lines depict the cross-shore components.

Conclusions

The year-long records of oceanographic conditions at three near-shore sites in Stefansson Sound near Prudhoe Bay describe two different regimes. During the summer months when there is open water and drifting sea ice the currents are wind driven, generally swift (>10 cm s^{-1}), highly variable, and strongly sheared. After landfast ice is established, the currents are decoupled from direct forcing by the wind and uncorrelated with the local wind field. There is also a substantial reduction in current magnitude (with speeds generally <10 cm s^{-1}), variability, and shear relative to the wind-driven regime. However, the current fluctuations are spatially coherent year round over at least 28 km. The low correlation between local winds and currents in winter suggests that other mechanisms are responsible for the low-frequency currents observed at this time of the year. These could be fluctuations in atmospheric pressure and/or by offshore oceanic motions. Both are of broad enough scale to account for the spatial coherence observed in the currents. For example, Aagaard [1984] and Aagaard and Roach [1990] have suggested that remotely forced oceanic motions could account for fluctuations in the flow over the Beaufort Shelf.

Our measurements suggest the possibility that in June, prior to the breakup of landfast ice, portions of Stefansson Sound might be influenced by under-ice river plumes that carry a large burden of suspended material that subsequently sinks to the bottom.

Finally, we note that our measurements have been made in Stefansson Sound, which is somewhat protected by a barrier island complex. There are wide and, in some places, relatively deep channels between these islands so that communication between the sound and offshore waters is not as restricted as elsewhere along the Beaufort coast. For example, Simpson Lagoon lies to the west of Prudhoe Bay and is bounded by a relatively extensive chain of barrier islands having fewer and shallower passes than those associated with the barrier islands offshore of Stefansson Sound. Moreover, Simpson Lagoon is shallower and narrower in width. We believe that flow conditions in Simpson Lagoon will be comparable to those measured in Stefansson Sound and that our measurements are probably representative of lagoon flows elsewhere along the North Slope. However, it is not clear if our measurements within Stefansson Sound reflect the magnitudes of currents beneath the landfast ice at locations seaward of the barrier islands.

Acknowledgements

Study Products

Portions of data collected and analyzed in this project were presented as follows:

Weingartner T.J. 2000. Beaufort Sea nearshore under-ice currents: Science, analysis and logistics, p. 75. *In* University of Alaska Coastal Marine Institute Annual Report No. 6. OCS Study MMS 2000-046, University of Alaska Fairbanks and USDOI, MMS, Alaska OCS Region.

Weingartner T.J. 2000. Beaufort Sea nearshore under-ice currents: Science, analysis and logistics, p. 37–41. *In* University of Alaska Coastal Marine Institute Annual Report No. 7. OCS Study MMS 2000-070, University of Alaska Fairbanks and USDOI, MMS, Alaska OCS Region.

Weingartner T.J. 2001. Beaufort Sea nearshore under-ice currents: Science, analysis and logistics. University of Alaska Coastal Marine Institute Annual Research Review, February 2001, Fairbanks.

Weingartner, T.J. 2001. Beaufort Sea nearshore under-ice currents: Science, analysis and logistics. MMS Information Transfer Meeting, April 2001, Anchorage.

Weingartner, T.J. 2001. Going to extremes: Buoyancy forcing on arctic continental shelves. Gordon Conference on Coastal Ocean Circulation, June 2001, New London, NH.

Dr. Weingartner was an invited speaker at this conference and presented some of the results from this project at the meeting.

Weingartner T.J., and S.R. Okkonen. 2001. Beaufort Sea nearshore under-ice currents: Science, analysis and logistics. Final Report. OCS Study MMS 2001-068, University of Alaska Coastal Marine Institute, University of Alaska Fairbanks and USDOI, MMS, Alaska OCS Region, 22 p.

References

Aagaard, K. 1984. The Beaufort undercurrent, p. 47–71. *In* P. Barnes and E. Reimnitz [eds.], The Alaskan Beaufort Sea: Ecosystems and Environment. Academic Press, New York.

Aagaard, K., and A.T. Roach. 1990. Arctic ocean–shelf exchange: Measurements in Barrow Canyon. J. Geophys. Res. 95:18163–18175.

Carmack, E.C., R.W. Macdonald and J. E. Papdakis. 1989. Water mass structure and boundaries in the Mackenzie Shelf Estuary. J. Geophys. Res. 94:18043–18055.

Chapman, D.C., and S.J. Lentz. 1994. Trapping of a coastal density front by the bottom boundary layer. J. Phys. Oceanogr. 24:1464–1479.

Davis, R.E. 1976. Predictability of sea surface temperature and sea level pressure anomalies over the North Pacific Ocean. J. Phys. Oceanogr. 6:249–266.

Dean, K.G., W. Stringer, K. Ahlnaes, S.C. Searcy and T. Weingartner. 1994. The influence of river discharge on the thawing of sea ice: Mackenzie River Delta: Albedo and temperature analysis. Polar Res. 13:83–94.

Kowalik, Z., and A.Y. Proshutinsky. 1994. The Arctic Ocean tides, p. 137–158. *In* O.M. Johannessen, R.D. Muench and J.E. Overland [eds.], The Polar Oceans and Their Role in Shaping the Global Environment. Geophys. Monogr. 85, Amer. Geophys. Union, Washington, DC.

Macdonald, R.W., E.C. Carmack, F.A. McLaughlin, K. Iseki, D.M. Macdonald and M.C. O'Brien. 1989. Composition and modification of water masses in the Mackenzie Shelf Estuary. J. Geophys. Res. 94:18057–18070.

Matthews, J.B. 1981. Observations of under-ice circulation in a shallow lagoon in the Alaskan Beaufort Sea. Ocean Manage. 6:223–234.

North, G.R., T.L. Bell and R.F. Cahalan. 1982. Sampling errors in the estimation of empirical orthogonal functions. Monthly Weath. Rev. 110:699–706.

Reimnitz, E., L. Toimil and P. Barnes. 1978. Arctic continental shelf morphology related to sea-ice zonation, Beaufort Sea, Alaska. Mar. Geol. 28:179–210.

Searcy, C., K. Dean and W. Stringer. 1996. A river–coastal sea ice interaction model: Mackenzie River Delta. J. Geophys. Res. 101:8885–8894.

Weingartner, T.J., D.J. Cavalieri, K. Aagaard and Y. Sasaki. 1998. Circulation, dense water formation, and outflow on the northeast Chukchi shelf. J. Geophys. Res. 103:7647–7661.

Weingartner, T.J., S. Danielson, Y. Sasaki, V. Pavlov and M. Kulakov. 1999. The Siberian Coastal Current: A wind- and buoyancy-forced arctic coastal current. J. Geophys. Res. 104:29697–29713.

Yankovsky, A.E., and D.C. Chapman. 1997. A simple theory for the fate of buoyant coastal discharges. J. Phys. Oceanogr. 27:1386–1401.